Scanner based on rotating optical wedges and its capabilities in airborne lidar

A.A. Tikhomirov, A.V. Beresnev, and A.A. Abramochkin

Institute of Optical Monitoring,
Siberian Branch of the Russian Academy of Sciences, Tomsk

Received January 12, 2000

In this paper we consider the characteristics and peculiarities of an airborne lidar scanner based on two optical wedges which can rotate in phase or in opposite directions (in antiphased). The parameters of the cycloid, the lidar optical axis follows in the case of cophased scanning, are analyzed. Possible scanning trajectories in the basic coordinate system are given for the case of antiphased rotation of wedges and at different positions of the scanning plane with respect to a flight direction (perpendicular, parallel, and at an arbitrary angle). The influence of flight parameters (altitude and velocity) and scanning parameters (angular rotation velocity and deflection of the lidar optical axis), as well as of the pulse repetition frequency on the density of laser pulse distribution over the sensed surface is estimated. The obtained results are applicable to scanners of other types and to space-based scanning lidars.

Introduction

A lidar system mounted aboard an aircraft allows remote sensing of the environment over territories of hundreds square kilometers,[1,2] as well as study of local formations in the atmosphere, hydrosphere, and Earth's surface from close distances. It is most suitable for real-time monitoring of the atmosphere and land on the regional scale. Besides, if the aircraft is equipped with a navigation system, measurement results can be referred to geographical coordinates.

By scanning over the objects under study with the optical axis of an airborne lidar allows the territory under study to be extended and provides the ability of sensing one object by several pulses. Omitting the case of directly tilting the lidar transceiver, the direction of the lidar optical axis can be changed in three ways: (i) by tilting or rotation of a steering mirror,[3,4] (ii) rotation of an optical wedge,[5] and (iii) use of a holographic diffraction grating.[6] Comparing the first and the second methods, it should be noted that the second one is preferable for several reasons: smaller size and mass and, consequently, lower angular momentum, no drive returns, lower degree of depolarization of the emitted and received radiation fluxes at polarization sensing, and wide capabilities in selection of scanning trajectories.

This paper discusses the capabilities of the wedge-based scanner for use in an airborne lidar.

Peculiarities of a wedge scanner

Regardless of the transceiving scheme of a monostatic lidar (coaxial or biaxial), a scanning element should be the same for the sensing and backscattered fluxes. This excludes additional misalignment of the optical axes of the transmitter and receiver in a medium sounded.

Figure 1 shows a scanner based on two optical wedges. The scanner was designed for the Makrel–2 lidar employing a biaxial transceiving system.[2,5] The transmitter and receiver apertures shown by dashed circles are completely described by the perimeter of a round wedge.

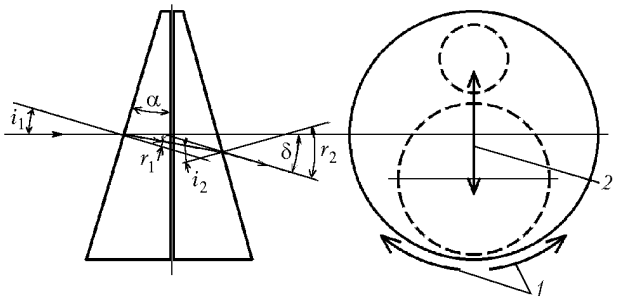

Fig. 1. Ray geometry in a wedge scanner: direction of the wedge rotation *1*, direction of ray scanning *2* at antiphased rotation of wedges; i_1 and i_2 are the angles of incidence; r_1 and r_2 are the angles of refraction; δ is the ray deflection from the initial direction.

There are two reasons for the use of two wedges. The first one is purely technical being connected with the complexity of manufacture of a high-quality optical wedge of more than 30 cm in diameter with the vertex angle α exceeding 16°. The other reason is technically even more important because of a possibility of obtaining different scanning regimes at different directions of rotation of individual wedges, and this can be done without special changes in the scanner drive kinematics.

0235-6880/00/04 376-08 $02.00

From the geometrical optics equations it is easy to derive the relation between the deflection angle δ of a ray and the angle of incidence i_1 on the surface of a wedge made of a material with the refractive index n and having the vertex angle 2α:

$$\delta = i_1 - 2\alpha + \arcsin\{n \sin[2\alpha - \arcsin(\sin i_1 / n)]\}. \quad (1)$$

Figure 2 shows the dependence of the deflection angle δ on the parameters α and n of a two-element wedge. It is characteristic that the maximum deflection corresponds to small incidence angles i_1. The scanner of the Makrel–2 lidar has the angles α and i_1 which are indicated by vertical dashed lines in Fig. 2. For the design reasons,[5] the case that $i_1 = \alpha$ is preferable. In this case, the optical axes of the transceiver are normal to the wedge interface (see Fig. 1), and the angle δ exceeds the angle α by more than 1°. The angle δ is restricted by the size of an illuminator or a hatch in the aircraft fuselage, through which the sensing is being carried out.

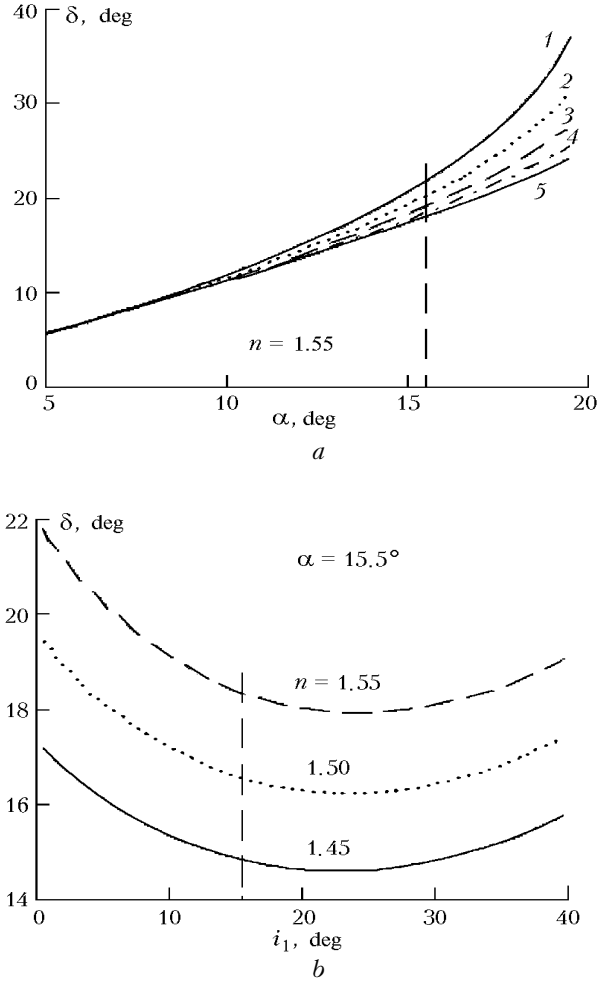

Fig. 2. Ray deflection angle vs. wedge parameters: angle α at different incidence angles (*a*): i_1 = 0.5° (*1*), 5° (*2*), 10° (*3*), 15° (*4*), and 20° (*5*); incidence angle at different refractive indices of glass (*b*).

Hereinafter, because of the small distance between the optical axes of the transmitter and receiver, we use a single term: lidar optical axis. When both wedges rotate in phase either clockwise or counterclockwise, this axis circumscribes a cone with the vertex angle 2δ. In the case of antiphased rotation, at which one wedge rotates clockwise, while the other one counterclockwise, the vertex angle of the double wedge for one period of rotation first decreases from 2α to 0 and then increases again up to 2α. As this takes place, the lidar optical axis scans in the plane perpendicular to the wedge interface with the maximum deflection from the initial direction by the angle ±δ. The direction of the scanning plane is set by the initial position of wedges – it is normal to wedge edges at the acute angles α, when these edges coincide. For the wedge arrangement shown in Fig. 1, the scanning direction at the antiphased rotation coincides with the vertical line shown by arrows in the right panel of the figure.

Possible scanning trajectories

Let us consider an airborne lidar flown along a straight line at a constant velocity V at an altitude H in the basic geotopical coordinate system $O_0X_gY_gZ_g$ (Ref. 7), which is rectangular and has the origin O_0 at some point on the Earth's surface. In this system, the axis O_0Y_g is directed along zenith, and the axes O_0X_g and O_0Z_g are usually referred to geographic coordinates. To describe the angular position and aircraft flight, a bound coordinate system $OXYZ$ is used. Its origin coincides with the aircraft's center of gravity, the axis OX is directed along the longitudinal axis of the aircraft, the axis OY lies in its symmetry plane and is directed upwards, and the axis OZ is directed toward the right-hand wing and is normal to the symmetry plane[7] (Fig. 3). The position of the lidar optical axis (sensing direction) is first set in the bound coordinate system of the aircraft and then, with the allowance for the aircraft movement parameters, is determined in the basic geotopical system. This allows sensing points (trajectory of the point where the optical axis meets the ground) to be set in coordinates on the Earth's surface.

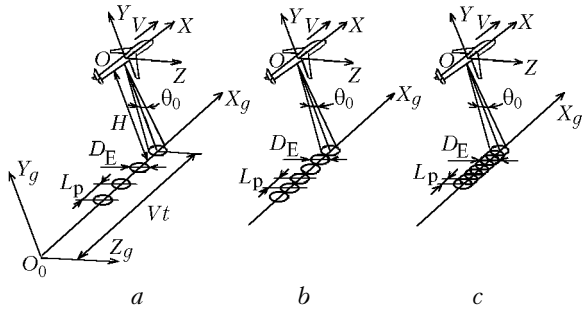

Fig. 3. Coordinate systems and parameters of sensing with no scanning: q = 2 (*a*), 1 (*b*), and 0.5 (*c*).

The main difference of airborne lidar sensing from the ground-based one is that the coordinates of the lidar optical axis in the basic coordinate system change continuously. As a result, each sensing event deals with a new object, and statistical information on a specific object can hardly be collected by means of multiple sensing. Besides, the sensing area is limited in space and on the plane by the trajectory of the aircraft flight. Scanning of the direction of the lidar optical axis at airborne sensing extends the territory under study and allows, under certain conditions, multiple sensing of one and the same object.

In the methodology of airborne sensing with a wedge scanner, we take into account the following parameters of the lidar: f_p is the pulse repetition rate, θ_0 is the angle of the laser beam divergence, ω_s is the angular velocity of rotation of the scanner wedges, δ is the angle of deflection of the lidar optical axis at scanning. Since aircraft is normally flown at altitudes above 100 m, which exceed their dimensions by an order of magnitude, the origin of the lidar optical axis can be considered coincident with the origin of the bound coordinate system. The lidar transceiver is set so that its optical axis in the bound coordinate system without scanning is parallel to the axis "$-OY$", that is, directed along nadir.

To simplify further analysis, we believe that at even and rectilinear flight of the aircraft the axes of the bound $OXYZ$ and basic $O_0X_gY_gZ_g$ coordinate systems are parallel, while the origin of the $OXYZ$ system is shifted from the origin O_0 along the axis O_0Y_g by the flight altitude H, and along the axis O_0X_g it shifts in time by Vt.

With no scanning, the diameter of a laser footprint on the surface is $D_E = H\theta_0$, and the distance between the centers of neighboring spots L_p (spatial period of sensing in the basic coordinate system) is determined by the flight speed V and the frequency f_p as $L_p = V/f_p$. Let us introduce the coefficient q of footprint distribution along the sensing trajectory. This coefficient can be written as

$$q = L_p/D_E = V/H\theta_0 f_p; \qquad (2)$$

it determines the spatial resolution of the airborne lidar. Thus, the following cases can be distinguished (see Fig. 3):

$$q = \begin{cases} > 1, & \text{isolated spots;} \\ = 1, & \text{tangent spots;} \\ < 1, & \text{overlapping spots.} \end{cases} \qquad (3)$$

Thus, under typical conditions of sensing $H = 1$ km, $f_p = 50$ Hz, $\theta_0 = 1.5$ mrad, and $V = 300$ km/h, we have $q = 1.1$, that is, almost continuous series of spots. As the flight speed increases or the pulse repetition frequency decreases, the distance between the spot centers increases. The third case in Eq. (3) is preferable, since at small D_E it allows a statistically significant data array on objects having uniform dimensions exceeding the laser spot diameter by an order of magnitude and more.

Let us now consider directions of scanning, which can be obtained with the use of a rotating wedge in a medium sounded, and the trajectories of the lidar optical axis end on the surface. In the bound coordinate system at a cophased rotation of two wedges, the lidar optical axis moves as a round cone generatrix, which describes a circle of radius $R_s = H\tan\delta$, where H is the flight altitude, and the minor axis of the ellipse of the conic section of the sensing ray at the distance $H/\cos\delta$ from the lidar is equal to $D_s = H\,\theta_0/\cos\delta$ (Fig. 4*a*). The linear speed with which the end of the optical axis moves on the surface $X_gO_0Z_g$ taking into account the scanning is as follows:

$$V_s = H\omega_s \tan\delta. \qquad (4)$$

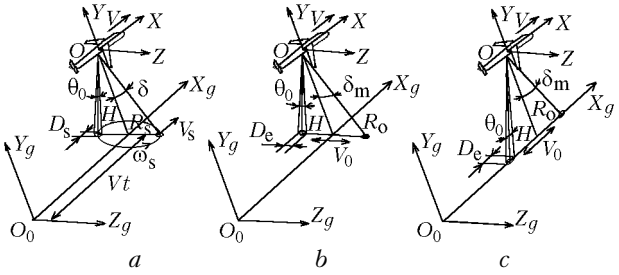

Fig. 4. Scanning and sensing parameters in bound coordinate system at cophased (*a*) and antiphased (*b*, *c*) rotation of wedges.

At scanning, the coefficient of distribution in the bound coordinate system is

$$q_s = \frac{V_s}{D_s f_p} = \frac{2\pi T_p \sin\delta}{\theta_0 T_s}. \qquad (5)$$

In contrast to Eq. (2), Eq. (5) shows that in the bound coordinate system at a cophased rotation the coefficient q_s is independent of the altitude H. However it is determined by the angular dimensions of the laser spot and by the ratio between the pulse repetition period T_p and the scanning period T_s. Using the above-listed lidar parameters $\theta_0 = 1.5 \cdot 10^{-3}$ mrad and $\delta = 16.965°$, we obtain $q_s = 1.22 \cdot 10^3\,(T_p/T_s)$. Thus, to obtain a continuous band of laser spots, the scanner rotation rate should be three orders of magnitude lower than the repetition frequency of laser pulses.

In the basic coordinate system $X_gO_0Z_g$, the lidar optical axis moves along a cycloid due to the aircraft motion. This cycloid is usually presented in a parametric form,[8] and for our case it is convenient to write the equation of cycloid as:

$$\begin{cases} X_g(t) = Vt \pm R_s \sin\omega_s t; \\ Z_g(t) = R_s \cos\omega_s t. \end{cases} \qquad (6)$$

The plus sign in the first equation of the system (6) corresponds to clockwise rotation of the optical axis.

The spatial period of the cycloid $L_c = 2\pi V/\omega_s$ is independent of the flight altitude H. In the plane $X_gO_0Z_g$ the maximum deflection of the lidar optical axis from the axis O_0X_g is equal to R_s, and the cycloid parameter is $\lambda = V_s/V$. At $\lambda > 1$, the cycloid is prolonged, that is, scanning follows the runback loops at a high angular rate ω_s (Fig. 5*a*). If ω_s and H are low ($V_s < V$), the cycloid becomes oblate and no runback scanning occurs (solid curve in Fig. 5*b*). At high ω_s and f_p, the runback scanning allows one to sense the same territory in a wide belt and thus to collect statistically significant data arrays for a certain period of time.

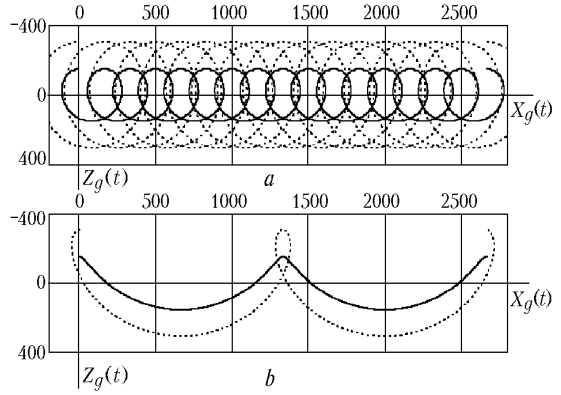

Fig. 5. The motion trajectories of the optical axis on the surface $X_gO_0Z_g$ at $H = 1000$ (– – –) and 500 m (——): $\omega_s = \pi$ rad/s, $L_c = 166.7$ m (*a*), $\omega_s = \pi/8$ rad/s, $L_c = 1333.3$ m (*b*). Distances at the axes are given in meters.

Analysis of Eq. (6) shows that at a limited range of flight speed V, it is more convenient to change the scanning trajectory by changing the scanner rotation rate ω_s. Figure 5 shows several possible cycloids and the corresponding scanning trajectories at $V = 300$ km/h. It is characteristic that as the altitude H increases, the linear speed V_s increases too, the cycloid becomes prolate, and the trajectory of optical axis motion on the surface becomes a runback one (see Fig. 5*b*).

In the basic coordinate system, the coefficient of distribution q_s determined by Eq. (5) changes due to the aircraft motion, since according to Eq. (6) the spatial period of sensing L_p between two pulses for the cycloid trajectory is the function of two coordinates X_g and Z_g and depends on the sum vector of the velocities V and V_s (see Fig. 4*a*). As a result, q_s becomes too complicated function of time, and it is difficult to derive a mathematical expression convenient for its analysis. In the next section, we present the results of numerical simulation of the distribution of laser spots over the surface $X_gO_0Z_g$.

Let us now consider the case of antiphased rotation of the scanner wedges. In the scanning plane passing through the axis "$-OY$" of the bound coordinate system, the deflection angle δ of the lidar optical axis changes as $\delta = \delta_m \cos \omega_s t$. When two wedges form a plane-parallel plate $\omega_s t = (2k + 1)\pi/2$, the optical axis coincides with the direction "$-OY$." The angle δ_m is calculated by Eq. (1), and the linear deflection R_o (see Figs. 4*b* and *c*) of the lidar optical axis from the axis "$-OY$" in the plane $X_gO_0Z_g$ changes as

$$R_o(t) = H \tan (\delta_m \cos \omega_s t). \qquad (7)$$

Then the linear speed of points on the lidar optical axis in the scanning plane (in the bound coordinate system) is

$$V_o(t) = \frac{dR_o(t)}{dt} = -\frac{\omega_s H \delta_m \sin \omega_s t}{\cos^2(\delta_m \cos \omega_s t)}. \qquad (8)$$

In contrast to Eq. (4), at the antiphased rotation of the wedges the linear speed of points on the lidar optical axis changes according to a harmonic law, close to the sinusoidal one, because at $\delta_m \cong 17°$ the denominator in Eq. (8) for the period T_s varies from 0.9 to 1.0. The major axis of the laser spot ellipse on the surface varies as

$$D_e(t) = \frac{\theta_0 H}{\cos^2\delta} = \frac{\theta_0 H}{[\cos (\delta_m \cos \omega_s t)]^2}. \qquad (9)$$

At the antiphased rotation of the wedges, the distribution coefficient is also a function of time

$$q_o(t) = \frac{|V_o(t)|}{D_e(t) f_p} = \frac{\delta_m \omega_s \cos \omega_s t}{\theta_0 f_p} \qquad (10)$$

in the bound coordinate system because the linear speed of the lidar optical axis changes; it achieves the maximum as it approaches the axis "$-OY$", that is, in the vicinity of this axis the density of the laser spots on the surface is the lowest and increases when approaching the deflection angle $\pm \delta_m$. To determine $q_o(t)$ in the basic coordinate system, one should substitute the absolute value of the sum vector of the velocities $V_o(t)$ and V instead of the velocity $V_o(t)$ in Eq. (10).

Since scanning in the bound coordinate system occurs in the plane passing through the axis "$-OY$," let us consider three typical cases of orientation of this plane in the basic coordinate system and the corresponding motion of the lidar optical axis end in the surface of the Earth or a cloud.

1. Scanning in the plane $Y_gO_0Z_g$ normal to the flight direction (see Fig. 4*b*). The equation of motion of the optical axis in a parametric form can be written as follows:

$$\begin{cases} X_g(t) = Vt; \\ Z_g(t) = H\tan(\delta_m \cos \omega_s t). \end{cases} \qquad (11)$$

As an example, Fig. 6 shows the trajectories of the lidar optical axis in the plane $X_gO_0Z_g$ for two altitudes and two wedge rotation rates. At such scanning, its motion in the surface or cloud top obeys a harmonic law.

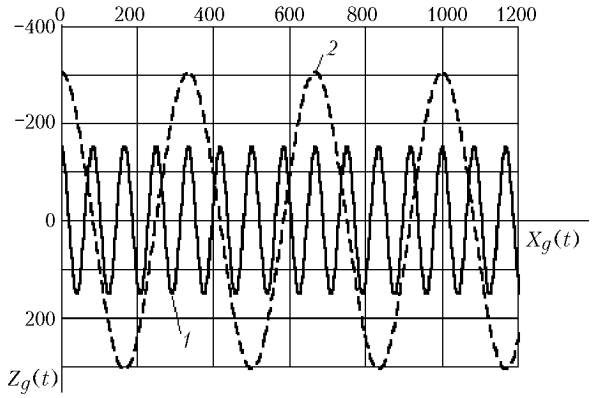

Fig. 6. Trajectories of the optical axis end on the surface at $H = 1000$ (– – –) and 500 m (——) at cross scanning: $\omega_s = 2\pi$ (*1*) and $\pi/2$ rad/s (*2*). Distances at the axes are given in meters.

2. Scanning in the plane $X_gO_0Y_g$ coincident with the flight direction (see Fig. 4*c*). In this case, the lidar optical axis moves only along the axis O_0X_g. Its equation of motion is

$$X_g(t) = Vt + H \tan (\delta_m \cos \omega_s t). \qquad (12)$$

It is characteristic that because the optical axis oscillates in the plane $X_gO_0Y_g$ it can repeatedly pass, depending on the ratio between ω_s, V, and H, through the same point on the surface $X_gO_0Z_g$. Figure 7 shows how the coordinate $X_g(t)$ of the lidar optical axis end on this surface changes in time for several scanning rates and flight altitudes. The slant straight line corresponds to the aircraft path or the motion of the projection of the axis OY along the axis O_0X_g. As is seen from this figure, at the trajectory *1* the lidar optical axis eight times passes through the point $X_g(t) = 0$. At the trajectory *2* the optical axis oscillates during 8 s about the point $X_g(t) \approx 330$ m, what allows an extended object to be observed for some finite time interval and some statistics on this object to be collected at a high pulse repetition frequency.

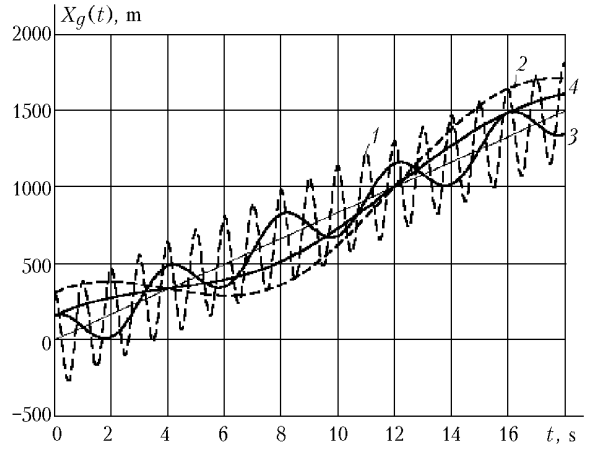

Fig. 7. Trajectories of the optical axis end on surface for $H = 1000$ (– – –) and 500 m (——) at longitudinal scanning: $\omega_s = 2\pi$ (*1*), $\pi/8$ (*2*), $\pi/2$ (*3*), and $\pi/8$ rad/s (*4*).

3. Scanning in the plane that makes the angle β with the flight direction. In this case, it is also convenient to present the coordinates of the of optical axis end in the plane $X_gO_0Z_g$ in a parametric form

$$\begin{cases} X_g(t) = Vt + H \tan (\delta_m \cos \omega_s t) \cos \beta; \\ Z_g(t) = H \tan (\delta_m \cos \omega_s t) \sin \beta. \end{cases} \qquad (13)$$

The trajectory of the lidar optical axis end at the particular angle $\beta = 45°$ is shown in Fig. 8. At certain flight parameters (H and V) and the rate ω_s the trajectory is a runback one, that is, it allows repeated sensing of an object during a finite time interval. If the optical axis moves along the trajectory *2*, at some sections the direction of its motion is normal to the flight direction.

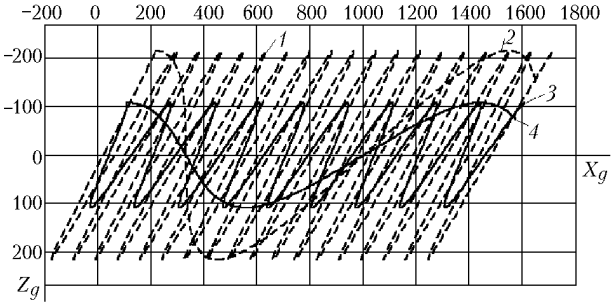

Fig. 8. Trajectories of the lidar optical axis end on the surface at $H = 1000$ (– – –) and 500 m (——) in scanning at the angle of 45° to flight direction: $\omega_s = 2\pi$ (*1*), $\pi/8$ (*2*), π (*3*), and $\pi/8$ rad/s (*4*). Distances at the axes are given in meters.

Thus, airborne laser sensing at the antiphased rotation of the wedges allows different trajectories of the lidar optical axis end in the basic coordinate system to be obtained by varying the flight altitude and the rate of the wedge rotation. Besides, although the aircraft moves, scanning of the lidar optical axis allows local objects to be sounded repeatedly by several pulses.

Spatial resolution

It was noted above that derivation of the mathematical equations for the coefficient of distribution of sensing areas q in the basic coordinate system in the form convenient for analysis is a problem because the spatial period of sensing L_p depends on both the scanning parameters and the flight speed. That is why we used the Mathcad package for numerical simulation of the distribution of laser spots along the trajectory of the lidar optical axis motion at a cophased and antiphased rotation of wedges for some values of f_p and ω_s at the constant values $H = 1000$ m, $\theta_0 = 1.5$ mrad, and $V = 300$ km/h. The characteristic results are shown in Figs. 9 – 12, where dots mark the track of laser spots on the plane $X_gO_0Z_g$. It should be noted that actual diameter of laser spots is almost an order of magnitude smaller than the bold dots shown in these figures.

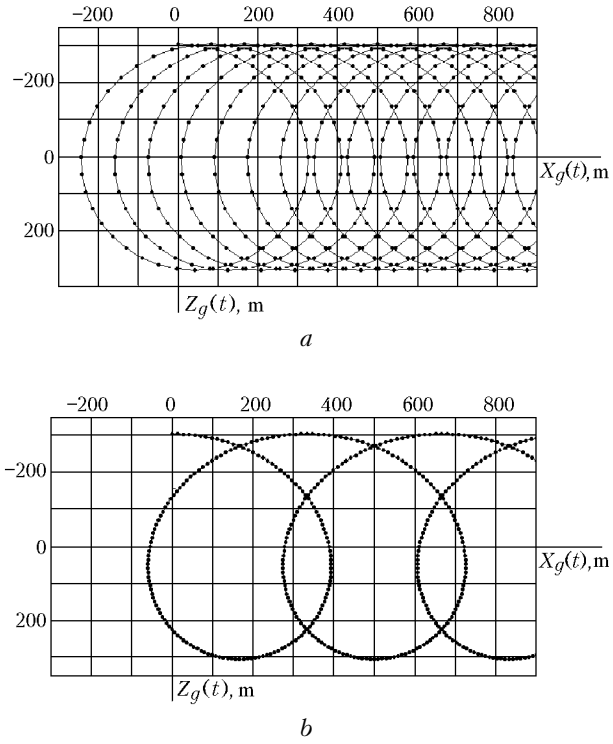

Fig. 9. Cophased clockwise rotation of wedges at f_p = 40 Hz: $\omega_s = 2\pi$ (*a*) and $\pi/2$ rad/s (*b*).

At a cophased rotation of the wedges (see Fig. 9), the largest spatial period L_p between the successive pulses is observed in the section of the cycloid, where the angle between the velocity vectors V and V_s is minimum (in the upper part of the trajectory). Conversely, in the runback (lower) section of the cycloid loop, where this angle is close to π (the velocity V is subtracted from the velocity V_s), the density of spots increases. The multiple increase of the frequency f_p leads to the corresponding multiple decrease of the spatial period L_p. As the angular rate ω_s (Fig. 9*b*) decreases, the linear velocity V_s of the lidar optical axis end decreases too, what also causes a decrease in the spatial period L_p and improves the spatial resolution of sensing along the trajectory of the lidar optical axis end. However, the total sensing resolution along the coordinate X_g decreases in this case, because cycloid loops become sparse. If one needs to uniformly cover a sensed territory by laser pulses within a belt of width $2R_s$ (see Fig. 4*a*), then the scanning and sensing parameters given in Fig. 9*a* are more suitable.

At the antiphased rotation of the wedges and scanning in the plane parallel to the basic plane $Y_gO_0Z_g$ (see Fig. 4*b*) and perpendicular to the flight direction ($\beta = 90°$), more uniform distribution of sensing pulses over the area is achieved at the scanning and sensing regimes corresponding to Fig. 10*a*. The density of dots increases at the ends of the sinusoid, at which the scanning speed $V_o(t)$ determined by Eq. (8) approaches zero. In this case, as for the cycloid, the density of laser spots on the surface is minimum in the areas close to the axis O_0X_g.

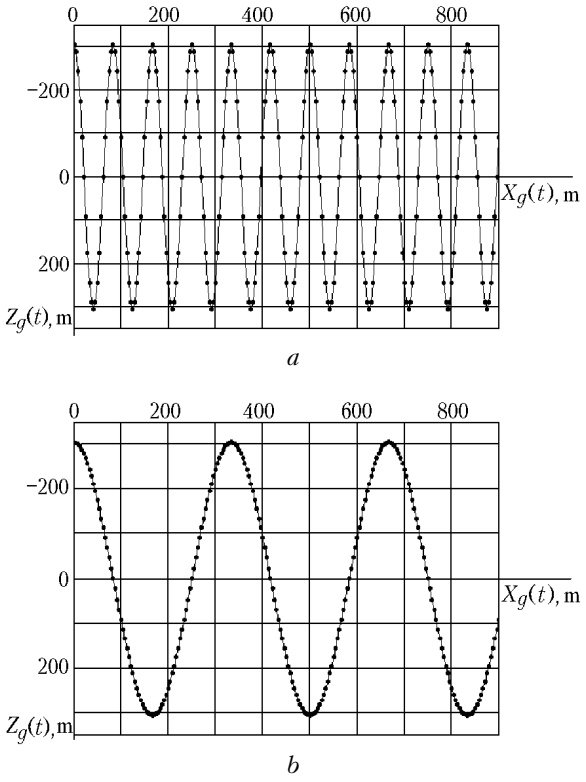

Fig. 10. Antiphased rotation of wedges ($\beta = 90°$) at f_p = 20 Hz: $\omega_s = 2\pi$ (*a*) and $\pi/2$ rad/s (*b*).

The slope of the scanning plane at an angle β to the flight direction decreases the scanning band by $\sin\beta$ times (see Fig. 11). However, the density of distribution of laser spots along the axes O_0X_g and O_0Z_g increases in this case over the entire scanning band. At a low rate ω_s, the case is possible that in a certain section of the trajectory, in the plane $X_gO_0Z_g$, the lidar optical axis moves along the axis O_0Z_g (see Fig. 11*b*). At this section of the trajectory, the values of the velocities V and $V_o(t)$ cos 45° are almost equal, but they are directed opposite to each other, and the lidar optical axis moves due to the component $V_o(t)$ sin 45°. In this case the coordinate $X_g(t)$ of the lidar optical axis changes, during a 2 s flight, from 330 to 336 m, that is, within four laser spot diameters, and the coordinate $Z_g(t)$ changes from –80.5 to +80.5 m, whereas the aircraft itself covers the distance of 167 m. The scale of laser spots in Fig. 11*b* is one fifth of their scale in the previous figure and now it is close to the actual value. Detailed analysis of the coefficient $q_o(t)$ at this section shows that it is ≈ 2.7, that is, to obtain tangent laser spots, the frequency f_p should be increased up to ≈ 60 Hz.

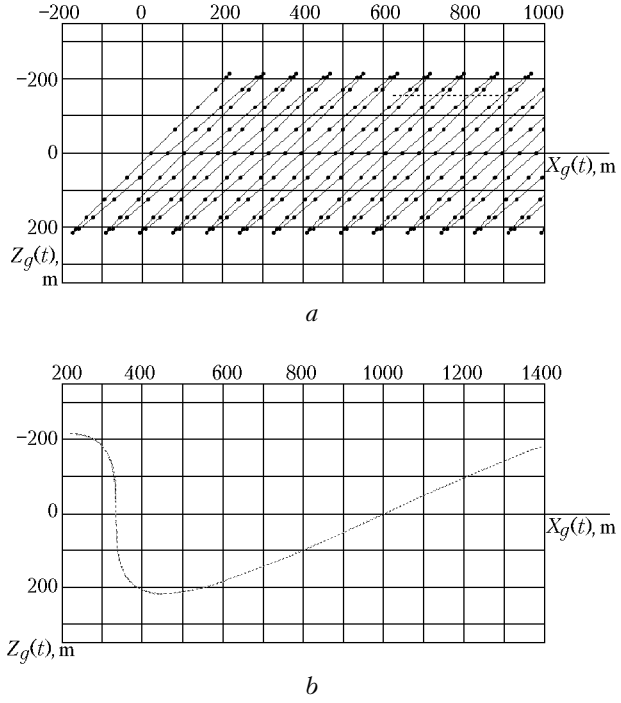

Fig. 11. Antiphased rotation of wedges ($\beta = 45°$) at $f_p = 20$ Hz: $\omega_s = 2\pi$ (*a*) and $\pi/8$ rad/s (*b*).

The results of scanning in the plane $X_g O_0 Y_g$ (see Fig. 4*c*) coincident with the flight direction ($\beta = 0°$) are shown in Fig. 12. In contrast to Fig. 7, here the abscissa shows the position of the origin of the bound coordinate system of the aircraft $X_g = Vt$. In this case, the projection of the flight trajectory is shown by a slant straight line, whereas deformed sinusoids show how the end of the lidar optical axis on the plane $X_g O_0 Z_g$ deflects from the projection of the aircraft center of gravity. Laser spots shown on the trajectory in Fig. 12*a* demonstrate that at a low frequency f_p the runback scanning may fail to ensure the laser pulses to arrive at the same points on the axis $O_0 X_g$, for example, the point with the coordinate $X_g = 0$. Only the increase of the pulse repetition frequency f_p up to 100 Hz, all other sensing and scanning parameters being the same as shown in Fig. 12*a*, provides that the lidar optical axis repeatedly crosses the same points at the axis $O_0 X_g$. The trajectory of laser spots shown in Fig. 12*b* by small dots for the wedge rotation rate $\omega_s = \pi/8$ rad/s shows their distribution in the scale close to the actual one. In this case, the area with the coordinate $X_g = (333 \pm 46)$ m is sensed during 8.2 s; the aircraft covers during this time more than 680 m distance. Decreasing the rate ω_s, we can find such its value that the lidar optical axis at longitudinal scanning is directed practically at the same point on the axis $O_0 X_g$ for a finite time interval.

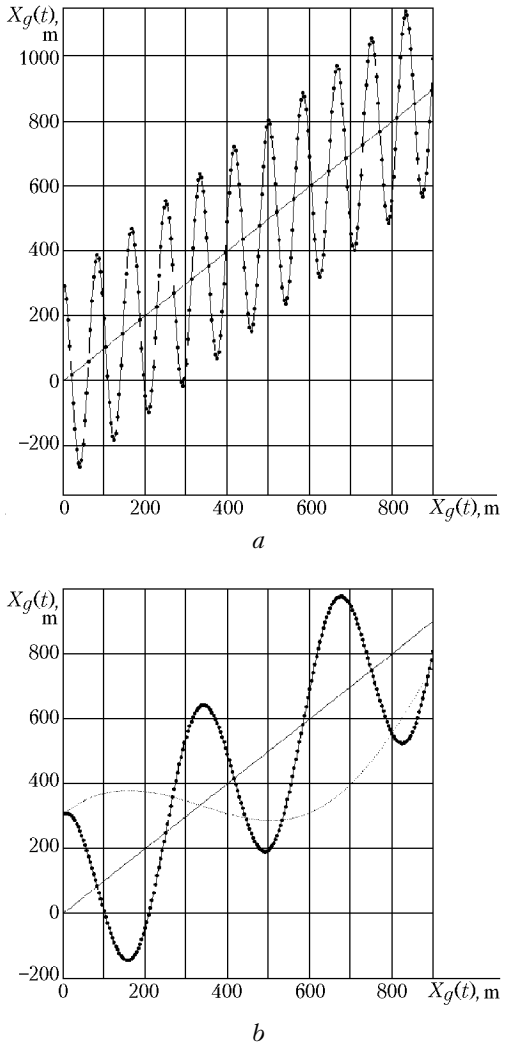

Fig. 12. Antiphased rotation of wedges ($\beta = 0°$) at $f_p = 20$ Hz: $\omega_s = 2\pi$ (*a*) and $\pi/2$ and $\pi/8$ rad/s (*b*). The slant straight line shows the flight trajectory.

Conclusion

The scanner based on two optical wedges provides for maximum deflection of the lidar optical axis up to $\delta_m = 17°$ and allows different scanning directions to be obtained both along the cone generatrix and in the plane oriented at any angle to the direction of motion. The maximum achievable rotation rate of the scanner wedges is $\omega_s = 2\pi$ rad/s at their total mass not exceeding 20 kg.

An airborne scanning lidar allows a territory to be sensed in a band of $2H \tan\delta_m$ wide with the spatial resolution dependent on the scanning parameters. On the whole, the density of distribution of laser pulses over the area $2Vt\,H \tan\delta_m$ depends on both the laser pulse repetition frequency f_p and the shape of the trajectory, the lidar optical axis circumscribes on the surface sounded. The trajectory itself depends on the

type of scanning (along a plane or a cone generatrix) and the scanning rate ω_s.

To obtain more uniform distribution of laser spots over the plane, it is worth using the trajectories of cycloid or a sinusoid at $\omega_s = 2\pi$ rad/s, which provide the maximum linear velocities of motion of the optical axis V_s [Eq. (4)] or $V_o(t)$ [Eq. (8)] at the flight altitude of 1000 m; these velocities exceed the flight velocity by more than order of magnitude (Figs. 9*a* and 10*a*). The increase of the pulse repetition frequency up to several kilohertzs with the use of diode pumped Nd:YAG lasers will allow practically continuous trajectory of laser spots to be obtained.[6]

The results presented here for the scanner based on the rotating optical wedges are applicable, with the needed corrections for angular rates, to a scanner based on rotating or oscillating mirrors.

The results obtained in this paper can also be interpolated to spaceborne lidar sensing with scanning. In this case, due to the significant increase of the flight height (by more than two orders of magnitude) the velocities V_s or $V_o(t)$ increase, but the flight velocity of a spacecraft also increases to the same degree (up to 7.8 km/s). The band $2H \tan\delta_m$ covered by lidar sensing also increases, so the density of distribution of laser pulses over a territory remains unchanged.

References

1. I.V. Samokhvalov and V.S. Shamanaev, "*Airborne lidars and their applications*," Dep. VINITI No. 2403–B88, March 29, 1988, Moscow (1988), 38 pp.
2. A.A. Tikhomirov and V.S. Shamanaev, in: *Regional Atmospheric Monitoring*. Part 2. *New Instruments and Measurement Methods* (SB RAS Publishing House, Tomsk, 1997), pp. 58–78.
3. M.F. Penny, R.H. Abbot, D.M. Phillips, et al., Appl. Opt. **25**, No. 13, 2046–2058 (1983).
4. S.P. Palm, S.H. Melfi, and D.L. Carter, Appl. Opt. **33**, No. 24, 5674–5681 (1994).
5. A.I. Abramochkin, V.V. Zanin, I.E. Penner, A.A. Tikhomirov, and V.S. Shamanaev, Opt. Atm. **1**, No. 2, 92–96 (1988).
6. G.K. Schwemmer, in: *Abstracts of Reports at 19th ILRC* (1998), Part 2, pp. 623–626.
7. I.G. Khivrich, N.F. Mironov, and A.M. Belkin, *Air Navigation* (Transport, Moscow, 1984), 328 pp.
8. I.N. Bronshtein and K.A. Semendyaev, *Mathematics Handbook for Engineers and Students of Technical Institutes* (State Physical and Mathematical Press, Moscow, 1962), 608 pp.